HHS Public Access

Author manuscript

J Am Chem Soc. Author manuscript; available in PMC 2018 October 04.

Published in final edited form as:

J Am Chem Soc. 2017 October 04; 139(39): 13640–13643. doi:10.1021/jacs.7b07979.

Direct Observation of Oxygen Rebound with an Iron-Hydroxide Complex

Jan Paulo T. Zaragoza[†,iD], **Timothy H. Yosca**[‡], **Maxime A. Siegler**[†], **Pierre Möenne-Loccoz**[§,iD], **Michael T. Green**[‡], and **David P. Goldberg**[*,†,iD]

[†]Department of Chemistry, The Johns Hopkins University, 3400 N Charles Street, Baltimore, Maryland 21218, United States

[‡]Department of Chemistry, University of California–Irvine, 1102 Natural Sciences II, Irvine, California 92697, United States

[§]Institute of Environmental Health, Oregon Health & Science University, Portland, Oregon 97239, United States

Abstract

The rebound mechanism for alkane hydroxylation was invoked over 40 years ago to help explain reactivity patterns in cytochrome P450, and subsequently has been used to provide insight into a range of biological and synthetic systems. Efforts to model the rebound reaction in a synthetic system have been unsuccessful, in part because of the challenge in preparing a suitable metal-hydroxide complex at the correct oxidation level. Herein we report the synthesis of such a complex. The reaction of this species with a series of substituted radicals allows for the direct interrogation of the rebound process, providing insight into this uniformly invoked, but previously unobserved process.

The selective hydroxylation of C–H bonds is a critical transformation for a wide range of biological processes, including oxidative metabolism, the detoxification of xenobiotics, and the biosynthesis of natural products. The same transformation is of widespread importance in organic synthesis, from the preparation of pharmaceuticals, to the synthesis of numerous specialty and commodity chemicals. Both heme and nonheme metalloenzymes carry out C–H hydroxylations with high efficiency and selectivity.[1a,b] In comparison, there are relatively

---

[*]**Corresponding Author**. dpg@jhu.edu.

ORCID

Jan Paulo T. Zaragoza: 0000-0002-2583-6571

Pierre Möenne-Loccoz: 0000-0002-7684-7617

David P. Goldberg: 0000-0003-4645-1045

ASSOCIATED CONTENT

Supporting Information

The Supporting Information is available free of charge on the ACS Publications website at DOI: 10.1021/jacs.7b07979.

Experimental details (PDF)

Data for $C_{91}H_{59}ClFeN_4$ (CIF)

Data for $C_{91}H_{60}FeN_4O$, C_5H_{12} (CIF)

The authors declare no competing financial interest.

Author Manuscript Author Manuscript Author Manuscript Author Manuscript

few synthetic complexes, especially with biologically compatible metal ions, that can mediate the same C–H hydroxylation chemistry.[1c,d] The canonical mechanism invoked for C–H hydroxylation is the so-called "rebound" mechanism, exemplified by cytochrome P450 (CYP) (Scheme 1). The initial step involves H atom abstraction from a C–H bond by a high-valent metal-oxo species, Compound-I (Cpd-I, $Fe^{IV}(O)(porph^{+\bullet})$), leading to protonated Compound-II (Cpd-II, $Fe^{IV}(OH)(porph)$), followed by "rebound" of the newly formed metal-bound hydroxide to the carbon radical to give the hydroxylated product and the one-electron-reduced $Fe^{III}(porph)$.[1e,f]

Efforts over the years have led to evidence that supports the rebound mechanism, including studies with radical clock probes,[1a] as well as myriad computational analyses.[1g] However, direct observation of the radical rebound step has been impossible because the initial C–H cleavage step is invariably rate-determining, making rebound invisible to spectroscopic interrogation. It was not until recently that one of us showed Cpd-I in CYP could be characterized spectroscopically,[1e] which did allow for direct study of the C–H cleavage step, but left the radical rebound step unobserved.

One way to overcome the problems associated with observing the rebound process is to independently prepare the rebound intermediate and examine its reactivity with well-defined organic radicals. However, this strategy has been unsuccessful to date because of the inherent difficulties in generating discrete, well-characterized Fe(OH) species at the correct redox level.[2] The putative rebound intermediate, i.e., protonated Cpd-II ($(Fe^{IV}OH)(porph)$), has predominantly been trapped and spectroscopically observed in heme proteins containing anionic axial ligands,[3] leading to a trianionic environment at the metal. To our knowledge, synthetic analogs of protonated Cpd-II remain unknown. We hypothesized that the corrole ligand, which presents a trianionic donor set without the need for an axial donor, could act to stabilize the key $[Fe(OH)]^{3+}$ state. Herein we report the development of an iron-hydroxide Cpd-II model complex, and demonstrate that it can be used for the direct interrogation of radical rebound reactions.

Part of the synthetic challenge to prepare an appropriate mononuclear Fe(OH) complex comes from the propensity of iron complexes to form Fe–O–Fe dimers. We hypothesized that the large steric encumbrance of the tris(2,4,6-triphenyl)-phenyl corrole ligand ($ttppcH_3$) shown in Figure 1 might prevent μ-oxo dimer formation. Metal-free $ttppcH_3$ was prepared via modification of a previous report.[4a] Metalation with $FeCl_2$ gave $Fe^{IV}Cl(ttppc)$ (**1**) as a brown solid (86%). The UV–visible and ^1H nuclear magnetic resonance (NMR) spectra of **1** are similar to those of other $Fe^{IV}(Cl)$ corroles.[4b] The structure for **1** was determined by X-ray diffraction (XRD), and the result is shown in Figure 1a. The Fe–N and Fe–Cl bond lengths (Table S3) are similar to those for $Fe^{IV}(Cl)(tpfc)$ (tris(pentafluoro)phenyl corrole).[4b]

Reaction of **1** with $Bu_4N^+OH^-$ was monitored by UV–vis spectroscopy. Upon addition of $Bu_4N^+OH^-$, the spectrum for **1** converted to a new species with a single Soret band at 403 nm (Figure S1). Monitoring the same reaction by ^1H NMR spectroscopy (Figure S2) revealed that paramagnetic **1** converts to a new species with a distinct pattern of paramagnetically shifted peaks. Mass spectrometry revealed a positive ion peak at m/z 1280.6, corresponding to $[Fe(ttppc)(OH)]^+$ (calcd m/z 1280.41). These data are consistent with formation of a new iron-hydroxide complex, **2**. Metathesis with LiOH in a two-phase H_2O/toluene mixture converted **1** to **2** on a larger scale, allowing for the isolation of **2** in the organic phase. The structure of $Fe^{IV}(OH)(ttppc)$ (**2**) was confirmed by XRD (Figure 1b). The Fe–O distance for the terminal hydroxide ligand is 1.857(3) Å. Although the hydrogen atom of the OH^- ligand could not be located in the difference Fourier maps, the Fe–O distance is too long for an unprotonated, terminal oxo ligand, and charge balance also requires protonation, presuming a formal +4 oxidation state for Fe.

Characterization of **1** and **2** in toluene at 110 K was carried out by resonance Raman (RR) spectroscopy. Excitation of **1** at 407 nm (Kr laser) gave rise to a prominent, resonance-enhanced peak at 343 cm^{-1}, which can be assigned to the Fe–Cl vibrational mode, and confirmed by ^{57}Fe isotopic substitution (Figure S5). This peak is not observed in the RR spectrum of **2**, whereas a new peak is detected at 576 cm^{-1}. Isotopic substitution of **2** via exchange with $H_2{}^{18}O$ gives **2**-^{18}O, and a new RR band at 555 cm^{-1} readily assigned to the $\nu(Fe–{}^{18}OH)$ mode on the basis of the 25 cm^{-1} downshift predicted for a diatomic Fe–O oscillator (Figure S6). The energy of this vibration falls in the same range as $\nu(Fe^{IV}–OH)$ seen for the heme protein chloroperoxidase ($\nu(Fe^{IV}–OH)$ = 565 cm^{-1}).[5] A Badger's rule analysis for a range of stretching frequencies normalized by reduced mass of the diatomic group[6] can be applied to predict an Fe–OH distance of 1.83 Å for **2**, which compares reasonably well with d(Fe–OH) = 1.857(3) Å obtained from XRD. The sensitivity of the $\nu(Fe^{IV}–OH)$ mode to H/D exchange via exposure of **2** to D_2O, which results in a 3 cm^{-1} upshift, supports the Fe–OH structure of **2**.

The synthesis of the Fe^{III} complex **3**, the expected product from the rebound process, was also targeted to obtain a spectroscopic benchmark. The cyclic voltammogram of **1** showstwo reversible redox couples at $E_{1/2}$ = +0.46, −0.64 V vs Fc^+/Fc (Figure S7a), and the latter couple can be assigned to the one-electron reduction of **1** to give $Fe^{III}(ttppc)$. Bulk chemical reduction of **1** was carried out by addition of $Cr(C_6H_6)_2$ ($E^{\circ\prime}$ = −1.15 V vs Fc^+/Fc, CH_2Cl_2) in ethyl acetate/diethyl ether, giving a new red species with λ_{max} = 415, 575, and 765 nm (Figure S8a). The red species was purified by chromatography to yield $Fe^{III}(OEt_2)_2(ttppc)$ (**3·2Et$_2$O**) as a red solid in good yield (81%). The UV–vis and ^1H NMR data for **3** are consistent with other Fe^{III} corroles.[4b]

We employed electron paramagnetic resonance (EPR) and Mössbauer spectroscopies to further characterize the electronic structures of complexes **1–3**. Corroles can behave as noninnocent ligands similar to porphyrins, complicating the oxidation state assignments of the central metal. The assessment of the electronic structures of $Fe^{IV}(corrole)(L)$ complexes has been particularly challenging, with the valence tautomers $Fe^{IV}(corrole)(L)/Fe^{III}(corrole^{+\bullet})(L)$, or a hybrid structure in between these canonical descriptions, as possibilities.[7] Complexes **1** and **2** are both EPR-silent (X-band, 16 K), whereas Mössbauer spectroscopy reveals quadrupole doublets with similar parameters (**1**: δ = 0.18 mm/s, ΔE_Q = 2.86 mm/s; **2**: δ = 0.13 mm/s, ΔE_Q = 2.21 mm/s) (Figure S9). The EPR spectrum for **3** shows an intense feature at g = 4.3 (Figure S8b) consistent with an intermediate-spin Fe^{III} (S = 3/2) corrole,[4b] and the Mössbauer spectrum (Figure S9c) shows a quadrupole doublet (δ = −0.09 mm s^{-1}, ΔE_Q = 4.00 mm s^{-1}) that is consistent with loss of magnetic splitting from intramolecular interactions, as seen for other Fe^{III} porphyrinoid compounds.[8] As seen for other Fe^{IV}

corroles, the Mössbauer and EPR data for **1** and **2** do not provide sufficient information to make a definitive assignment between Fe^{IV}(corrole)(L) or Fe^{III}($corrole^{+\bullet}$)(L) descriptions. However, the data are fully consistent with **1** and **2** being one redox level above the Fe^{III} complex **3**, which is the key feature required to initiate studies on the rebound process.

Complex **2** was examined in reactions with carbon-centered radicals (R·). Trityl radical ($Ph_3C\cdot$) is relatively stable in organic solutions, in equilibrium with its dimeric state (Gomberg's dimer): $2\ Ph_3C\cdot \rightleftharpoons (Ph_3C)_2$ (~2% $Ph_3C\cdot$ at 23 °C).[9] Reaction of Fe^{IV}(OH)(ttppc) with excess Gomberg's dimer in toluene at 23 °C resulted in the rapid, isosbestic conversion of Fe^{IV}(OH)(ttppc) to Fe^{III}(ttppc) by UV–vis (Figure S10). ^1H NMR spectroscopy (Figure S11) and gas chromatography (GC) (Figure S15a) showed that Ph_3COH (trityl alcohol) was formed in good yield (77%). Isotopic labeling of **2** was carried out by exchange with excess $H_2{}^{18}O$ under biphasic conditions and confirmed by mass spectrometry. Reaction of Fe^{IV}(^{18}OH)-(ttppc) with $Ph_3C\cdot$ led to $Ph_3C^{18}OH$ with 57% incorporation of ^{18}O (Figure S16). Taken together, these data show conclusively that OH is transferred from **2** to the trityl radical in a rebound process.

Insight into the mechanism of the rebound process was obtained by examination of a series of trityl derivatives, (p-X-C_6H_4)$_3$C· (X = OMe, tBu, Ph, Cl), in which the electron-donating properties of the X substituent was varied (Figure 2a). These derivatives exist exclusively as monomers in solution. Initial studies began with the *p*-tBu derivative. Reaction of (p-tBu-C_6H_4)$_3$C· with **2** gave the expected rebound products, **3** and (p-tBu-C_6H_4)$_3$COH, in good yields (Figure S13, S15b). Monitoring this reaction by UV–vis under pseudo-first-order conditions (Figure 2b) yielded a pseudo-first-order rate constant (k_{obs}), and a plot of k_{obs} versus [(p-tBu-C_6H_4)$_3$C·] was linear, whose slope gave a second-order rate constant of 49(1) $M^{-1}\ s^{-1}$. Second-order rate constants for the other substituted trityl radicals were determined similarly, ranging from 12.6(1) to 357(4) $M^{-1}\ s^{-1}$ for the methoxy derivative (Table S4).

A plot of log k versus $3\sigma^{+}_{para}$, where k is the second order rate constant and σ^{+}_{para} is the Hammett parameter for the *para*-X substituents, is shown in Figure 2c. A linear correlation is obtained ($r^2 = 0.99$), but the magnitude of the slope ($\rho = -0.55$) is small, suggesting only small charge separation in the transition state. For comparison, H atom transfer reactions between alkoxyl radicals and phenols (RO· + HOAr → ROH + ·OAr) also show small ρ values, and are described as proceeding through charge neutral transition states.[10]

The redox potentials (E_{ox}) for the (p-X-C_6H_4)$_3C^{+/\bullet}$ couples range from 0.00 to −0.58 V versus $Fc^{+/0}$ (CH_3CN). With the exception of the −Cl derivative (E_{ox} = 0.00 V), these values are lower than the redox potential for **2** (−0.11 versus $Fc^{+/0}$) measured by cyclic voltammetry (Figure S7b), making electron-transfer (ET) from the radicals to **2** an exergonic process. The ET process for the −Cl derivative is endergonic by 2.5 kcal/mol. To determine the involvement of ET in the rebound mechanism, a Marcus plot of $(RT/F)\ln(k)$ vs E_{ox} was constructed (Figure 2d). The Marcus cross-relation indicates that a slope of ~ −0.5 is expected for a simple, rate-limiting ET process.[11] The Marcus plot in Figure 2d reveals a linear correlation for the rebound reaction, but the slope is small (−0.15). This slope can be compared to the small slope (−0.05) seen for the reaction of cumylperoxyl radical and phenols, which is a good model of a concerted H atom transfer, as opposed to ET-type, mechanism.[12a,b] In contrast, Fujii has reported large slopes (0.60–0.68) for aromatic hydroxylation of benzene derivatives by $Fe^{IV}(O)(porph^{+\bullet})$ complexes. Simple outer-sphere ET for these reactions was ruled out based on endergonic $\Delta G°_{ET}$ values, but the large Marcus slopes pointed to an ET pathway that was coupled to a subsequent favorable C–O bond formation step.[12c]

With the data now in hand from the direct examination of a radical rebound reaction, we can suggest a straightforward mechanistic paradigm to assess the rebound step, in analogy with H atom transfer. HAT proceeds in an approximately concerted fashion, or in more of a stepwise one in which the ET/PT steps are coupled to varying degrees. The rebound mechanism can be parsed in a similar model, as shown in Figure 3a, in which rebound can occur via a concerted pathway, or electron-transfer and “cation transfer” (CT) steps. The Hammett and Marcus plots in Figures 2c,d indicate that the radical rebound reactions for **2** follow a concerted (diagonal path, Figure 3a), as opposed to “ET/CT” type of mechanism, in which C–O bond formation occurs concomitant with reduction of the iron complex. Thus, the transition state of the concerted rebound reaction is likely closer to the charge neutral structure shown in Figure 3b. Although **2** is sterically crowded, examination of a space-filling model of **2** (Figure S23) suggests that there is space for the trityl radical to combine with the FeOH above the pyrrole–pyrrole bond.

The mechanism of action for heme and nonheme oxygenases, as well as related transition metal catalysts, has been described in the framework of the rebound process shown in Scheme 1 for over 40 years. However, until now, the critical rebound step could not be observed and studied directly. In this report, we have described the first direct examination of a rebound hydroxylation, in which a well-defined Fe(OH) porphyrinoid complex is reacted with a series of carbon radicals. A key to this study was the use of a corrole ligand to isolate an Fe(OH) complex that is at the same oxidation level as the Cpd-II intermediate in heme enzymes. Such a species was previously unknown in porphyrinoid models of heme enzymes. The kinetic measurements provide a mechanistic assessment of the radical hydroxylation step, leading to a model for the rebound process that has both concerted and stepwise pathways, analogous to the well-known paradigm for HAT. Taken together, the data point to a more concerted process for rebound. With the precedent established here, the factors that favor and control rebound hydroxylation over other pathways, such as desaturation,[13a,b] halogenation,[13c,d] or radical cage escape,[13e] may now be amenable to direct interrogation.

Supplementary Material

Refer to Web version on PubMed Central for supplementary material.

Acknowledgments

The authors acknowledge support by the NIH (Grant GM101153 to D.P.G.). J.P.T.Z. thanks JHU for the Glen E. Meyer ’39 Fellowship. We also thank Dr. R. Baglia for helpful discussions, and T. Pangia for the synthesis of some compounds.

Author Manuscript Author Manuscript Author Manuscript Author Manuscript

References

1. (a) Ortiz de Montellano PR. Chem. Rev. 2010; 110:932. [PubMed: 19769330] (b) Kovaleva EG, Lipscomb JD. Nat. Chem. Biol. 2008; 4:186. [PubMed: 18277980] (c) Chen MS, White MC. Science. 2007; 318:783. [PubMed: 17975062] (d) Kudrik EV, Afanasiev P, Alvarez LX, Dubourdeaux P, Clémancey M, Latour J-M, Blondin G, Bouchu D, Albrieux F, Nefedov SE, Sorokin AB. Nat. Chem. 2012; 4:1024. [PubMed: 23174983] (e) Rittle J, Green MT. Science. 2010; 330:933. [PubMed: 21071661] (f) Huang X, Groves JT. JBIC, J. Biol. Inorg. Chem. 2017; 22:185. [PubMed: 27909920] (g) Shaik S, Kumar D, de Visser SP, Altun A, Thiel W. Chem. Rev. 2005; 105:2279. [PubMed: 15941215]
2. (a) Boaz NC, Bell SR, Groves JT. J. Am. Chem. Soc. 2015; 137:2875. [PubMed: 25651467] (b) Hill EA, Weitz AC, Onderko E, Romero-Rivera A, Guo Y, Swart M, Bominaar EL, Green MT, Hendrich MP, Lacy DC, Borovik AS. J. Am. Chem. Soc. 2016; 138:13143. [PubMed: 27647293]
3. Yosca TH, Langston MC, Krest CM, Onderko EL, Grove TL, Livada J, Green MT. J. Am. Chem. Soc. 2016; 138:16016. [PubMed: 27960340] Yosca TH, Rittle J, Krest CM, Onderko EL, Silakov A, Calixto JC, Behan RK, Green MT. Science. 2013; 342:825. [PubMed: 24233717] Green MT, Dawson JH, Gray HB. Science. 2004; 304:1653. [PubMed: 15192224] A neutron diffraction study provided evidence for a protonated Cpd-II in a His-ligated ascorbate peroxidase. See: Kwon H, Basran J, Casadei CM, Fielding AJ, Schrader TE, Ostermann A, Devos JM, Aller P, Blakeley MP, Moody PCE, Raven EL. Nat. Commun. 2016; 7:13445. [PubMed: 27897163]
4. (a) Liu H-Y, Yam F, Xie Y-T, Li X-Y, Chang CK. J. Am. Chem. Soc. 2009; 131:12890. [PubMed: 19737012] (b) Simkhovich L, Mahammed A, Goldberg I, Gross Z. Chem. - Eur. J. 2001; 7:1041. [PubMed: 11303864]
5. Stone KL, Behan RK, Green MT. Proc. Natl. Acad. Sci. U. S. A. 2006; 103:12307. [PubMed: 16895990]
6. Spaeth AD, Gagnon NL, Dhar D, Yee GM, Tolman WB. J. Am. Chem. Soc. 2017; 139:4477. [PubMed: 28319386]
7. (a) Walker FA, Licoccia S, Paolesse R. J. Inorg. Biochem. 2006; 100:810. [PubMed: 16519943] (b) Ye S, Tuttle T, Bill E, Simkhovich L, Gross Z, Thiel W, Neese F. Chem. - Eur. J. 2008; 14:10839. [PubMed: 18956397]
8. Leeladee P, Jameson GNL, Siegler MA, Kumar D, de Visser SP, Goldberg DP. Inorg. Chem. 2013; 52:4668. [PubMed: 23527920]
9. Trityl radical has been employed to study analogous NR transfer reactions from Cu- and Fe-N(H)Ar species. See: Jang ES, McMullin CL, Käß M, Meyer K, Cundari TR, Warren TH. J. Am. Chem. Soc. 2014; 136:10930. [PubMed: 24940616] Iovan DA, Betley TA. J. Am. Chem. Soc. 2016; 138:1983. [PubMed: 26788747]
10. Colclough N, Smith JRL. J. Chem. Soc., Perkin Trans. 2. 1994; 2:1139.
11. Marcus RA, Sutin N. Biochim. Biophys. Acta, Rev. Bioenerg. 1985; 811:265.
12. (a) Osako T, Ohkubo K, Taki M, Tachi Y, Fukuzumi S, Itoh S. J. Am. Chem. Soc. 2003; 125:11027. [PubMed: 12952484] (b) Lee JY, Peterson RL, Ohkubo K, Garcia-Bosch I, Himes RA, Woertink J, Moore CD, Solomon EI, Fukuzumi S, Karlin KD. J. Am. Chem. Soc. 2014; 136:9925. [PubMed: 24953129] (c) Asaka M, Fujii H. J. Am. Chem. Soc. 2016; 138:8048. [PubMed: 27327623]
13. (a) Grant JL, Mitchell ME, Makris TM. Proc. Natl. Acad. Sci. U. S. A. 2016; 113:10049. [PubMed: 27555591] (b) Rettie AE, Rettenmeier AW, Howald WN, Baillie TA. Science. 1987; 235:890. [PubMed: 3101178] (c) Wong SD, Srnec M, Matthews ML, Liu LV, Kwak Y, Park K, Bell CB III, Alp EE, Zhao J, Yoda Y, Kitao S, Seto M, Krebs C, Bollinger JM, Solomon EI. Nature. 2013; 499:320. [PubMed: 23868262] (d) Galonic DP, Barr EW, Walsh CT, Bollinger JM, Krebs C. Nat. Chem. Biol. 2007; 3:113. [PubMed: 17220900] (e) Cho K-B, Hirao H, Shaik S, Nam W. Chem. Soc. Rev. 2016; 45:1197. [PubMed: 26690848]

Author Manuscript Author Manuscript Author Manuscript Author Manuscript

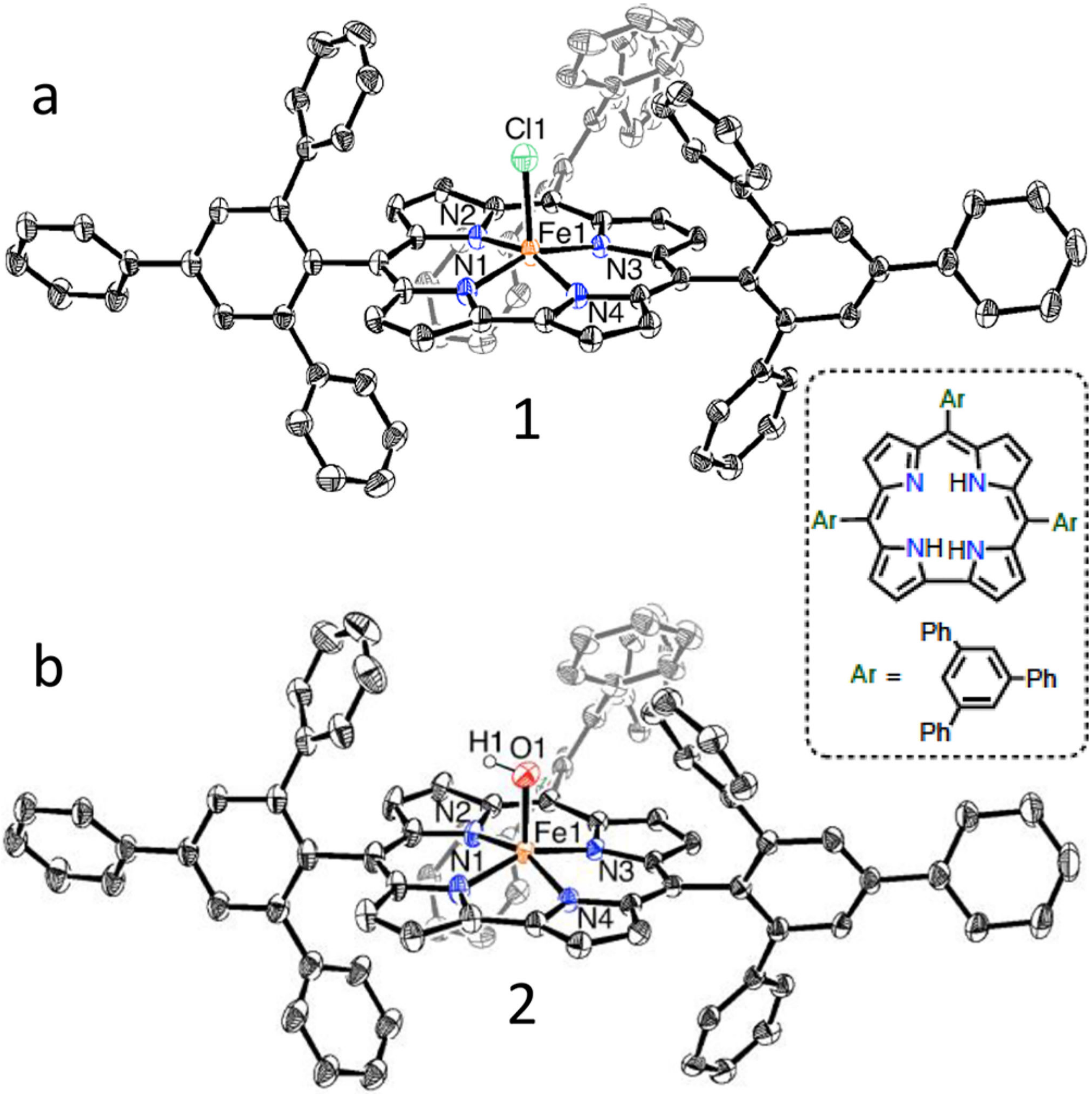
a
Cl1
N2
Fe1
N1
N3
N4
1
Ar
N
HN
Ar
Ar
NH
HN
Ph
Ar =
Ph
Ph
b
H1
O1
N2
Fe1
N1
N3
N4
2

Figure 1.
Displacement ellipsoid plots (35% probability level) for the molecular structures of (a) **1** and (b) **2** at 110(2) K. Hydrogen atoms, except for H(1) in **2**, omitted for clarity. Inset: structure of the metal-free corrole ligand used in this study.

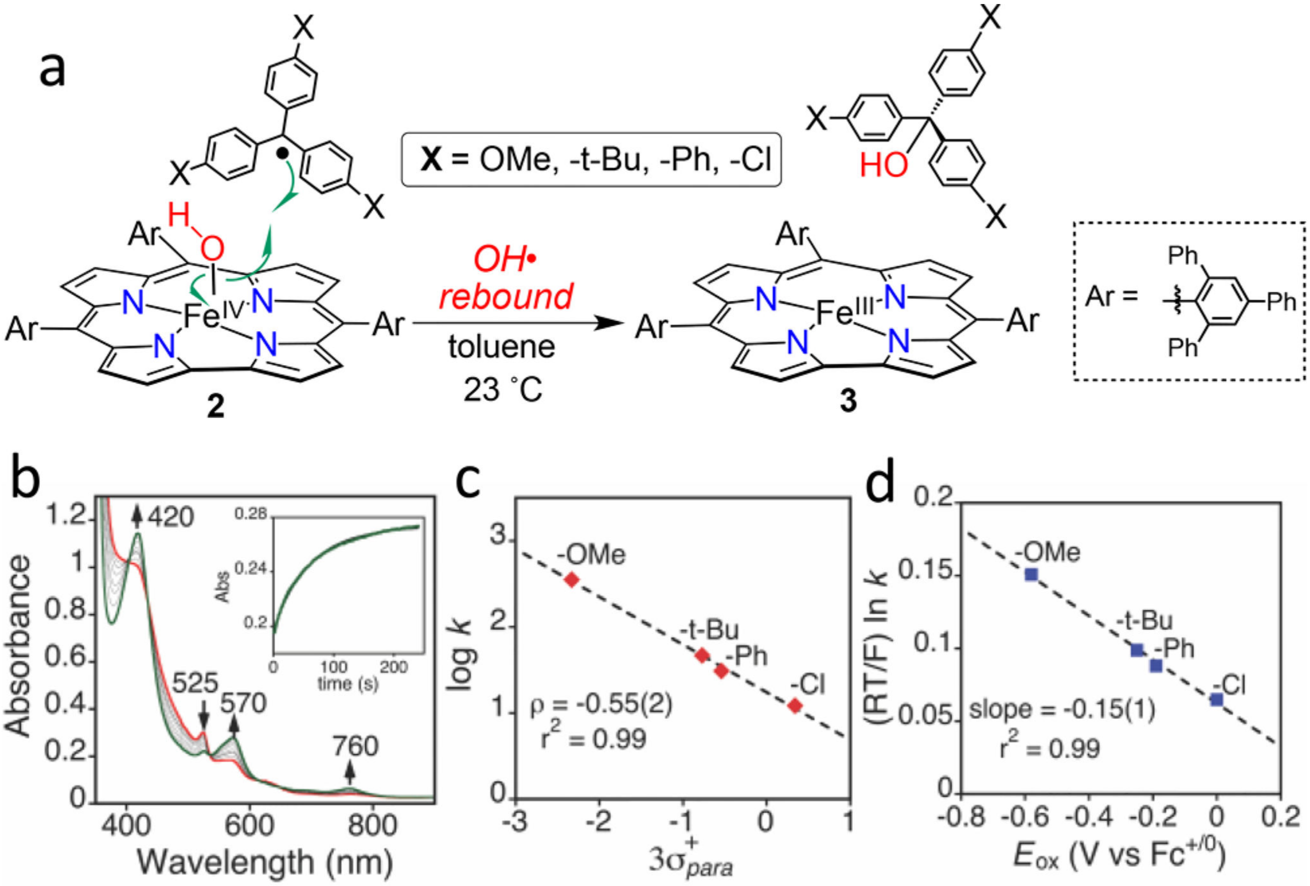

Figure 2.

(a) Oxygen rebound reaction for **2** with *para*-X-substituted trityl radicals. (b) Time-resolved UV–vis spectral changes observed upon addition of (p-tBu-$C_6H_4)_3C$· (0.33 mM) to **2** (20 μM) (red line, *t* = 0.5 s) to form **3** (green line, *t* = 220 s) in toluene at 23 °C. Inset: changes in absorbance for 570 nm vs time. (c) Hammett plot and (d) Marcus plot.

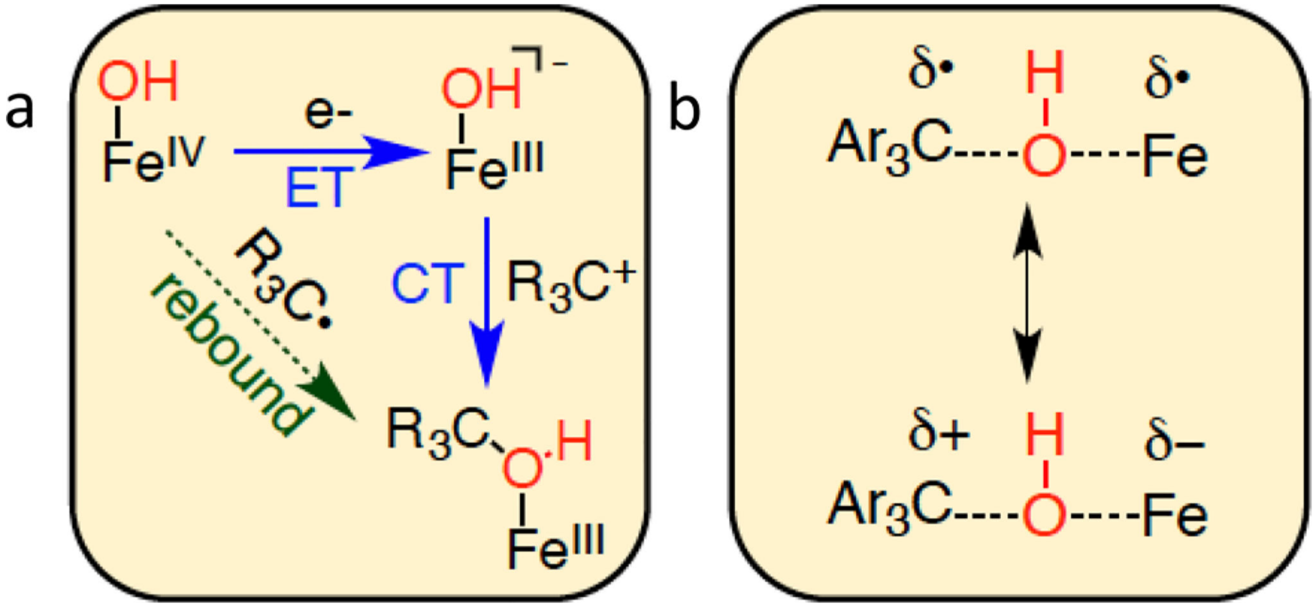
a
OH
Fe^IV
e-
ET
OH
Fe^III
CT
R3C+
R3C•
rebound
R3C
O
H
Fe^III
b
δ•
H
δ•
Ar3C----O----Fe
δ+
H
δ–
Ar3C----O----Fe

Figure 3.

(a) Scheme depicting concerted and separated ET/CT steps for radical rebound. (b) Charge separation in the transition state of the rebound reaction.

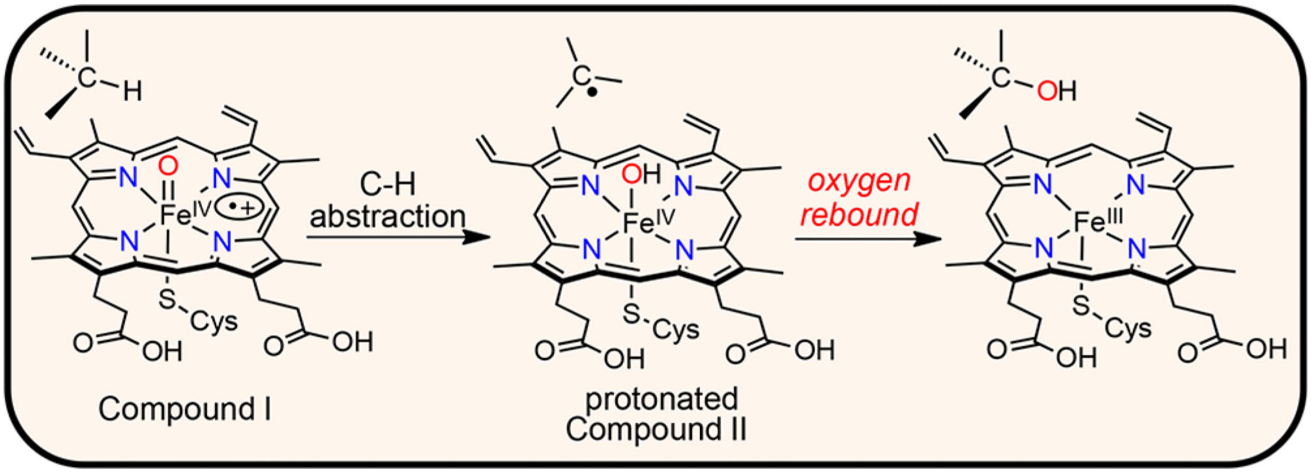
C-H
abstraction
oxygen
rebound
Compound I
protonated
Compound II
Fe^{IV}
Fe^{IV}
Fe^{III}
S-Cys
OH

Scheme 1.
So-Called “Rebound” Mechanism